Staphylococcus aureus Sortase Transpeptidase SrtA: Insight into the Kinetic Mechanism and Evidence for a Reverse Protonation Catalytic Mechanism†

Brenda A. Frankel,‡ Ryan G. Kruger,‡ Dana E. Robinson,§ Neil L. Kelleher,§ and Dewey G. McCafferty*,‡

Department of Biochemistry and Biophysics and Johnson Research Foundation, University of Pennsylvania School of Medicine, Philadelphia, Pennsylvania 19104-6059, and Department of Chemistry, University of Illinois, Urbana, Illinois 61801

Received January 24, 2005; Revised Manuscript Received May 30, 2005

ABSTRACT: The *Staphylococcus aureus* transpeptidase SrtA catalyzes the covalent attachment of LPXTG-containing virulence and colonization-associated proteins to cell-wall peptidoglycan in Gram-positive bacteria. Recent structural characterizations of staphylococcal SrtA, and related transpeptidases SrtB from *S. aureus* and *Bacillus anthracis*, provide many details regarding the active site environment, yet raise questions with regard to the nature of catalysis and active site cysteine thiol activation. Here we re-evaluate the kinetic mechanism of SrtA and shed light on aspects of its catalytic mechanism. Using steady-state, pre-steady-state, bisubstrate kinetic studies, and high-resolution electrospray mass spectrometry, revised steady-state kinetic parameters and a ping-pong hydrolytic shunt kinetic mechanism were determined for recombinant SrtA. The pH dependencies of kinetic parameters k_{cat}/K_m and k_{cat} for the substrate Abz-LPETG-Dap(Dnp)-NH_2 were bell-shaped with pK_a values of 6.3 ± 0.2 and 9.4 ± 0.2 for k_{cat} and 6.2 ± 0.2 and 9.4 ± 0.2 for k_{cat}/K_m. Solvent isotope effect (SIE) measurements revealed inverse behavior, with a $^{D_2O}k_{cat}$ of 0.89 ± 0.01 and a $^{D_2O}(k_{cat}/K_m)$ of 0.57 ± 0.03 reflecting an equilibrium SIE. In addition, SIE measurements strongly implicated Cys184 participation in the isotope-sensitive rate-determining chemical step when considered in conjunction with an inverse linear proton inventory for k_{cat}. Last, the pH dependence of SrtA inactivation by iodoacetamide revealed a single ionization for inactivation. These studies collectively provide compelling evidence for a reverse protonation mechanism where a small fraction (ca. 0.06%) of SrtA is competent for catalysis at physiological pH, yet is highly active with an estimated k_{cat}/K_m of $>10^5$ M^{-1} s^{-1}.

The pathogenesis and infectivity of Gram-positive bacteria are mediated by a multitude of surface protein virulence factors such as MSCRAMMs[1] (microbial surface components recognizing adhesive matrix molecules) which aid in adhesion to host endothelial tissues, and protein A which functions in immune system evasion. Despite a variety of functions, these virulence factors are characterized by a common C-terminal cell-wall sorting signal (cws) that enables their covalent attachment to the peptidoglycan layer of Gram-positive bacteria through a reaction catalyzed by the sortase family of transpeptidases (*1*). In *Staphylococcus aureus*, sortase isoform SrtA intercepts surface proteins as they are being secreted through the cytoplasmic membrane, cleaves within the C-terminal LPXTG cws between threonine and glycine, and subsequently transfers the N-terminal domain to the amino terminus of the pentaglycine (Gly_5) cross-linking spacer from the peptidoglycan biosynthetic intermediate branched Lipid II (Figure 1) (*2*, *3*). Once covalently attached to branched Lipid II, this intermediate becomes polymerized into mature peptidoglycan through the combined action of transglycosylases and transpeptidases. The ubiquitous nature of this mechanism is evidenced by the identification of closely related sortase orthologs and the conservation of myriad LPXTG-containing substrates in the genomes of all Gram-positive bacteria sequenced to date (*4*, *5*).

In addition to SrtA, isoform SrtB has been identified in the genome of *S. aureus*. While *S. aureus* SrtB appears to play a specialized role in late-stage infection by anchoring NPQTN-containing proteins involved in host heme iron sequestration and intracellular transport (*6*), numerous lines of genetic evidence have shown that SrtA plays a critical dominant role in pathogenesis by modulating surface protein attachment of LPXTG-containing proteins that are responsible for bacterial attachment to host tissues and evasion of host immune defenses (*7*−*13*). Collectively, these studies suggest that in the absence of SrtA activity, bacteria have a drastically reduced capacity to establish persistent infections in host organisms. SrtA inhibitors may therefore be effective in treating Gram-positive bacterial infections by altogether preventing or significantly reducing the rate of infection onset.

Several inhibitors of SrtA have been reported, including peptide derivatives which lack potential for use as in vivo

† This work was supported by NIH Grants AI46611 (to D.G.M.) and GM067725 (to N.L.K.) and an NSF Predoctoral Fellowship to B.A.F.

* To whom correspondence should be addressed: Department of Biochemistry and Biophysics, University of Pennsylvania School of Medicine, 905A Stellar-Chance Building, 422 Curie Blvd., Philadelphia, PA 19104-6059. Phone: (215) 898-7619. Fax: (215) 573-8052. E-mail: deweym@mail.med.upenn.edu.

‡ University of Pennsylvania School of Medicine.

§ University of Illinois.

[1] Abbreviations: Abz, aminobenzoic acid; Dap, diaminopropionic acid; Dnp, dinitrophenyl; cws, cell-wall sorting signal; MSCRAMMs, microbial surface components recognizing adhesive matrix molecules; GN, *N*-acetylglucosamine; MN, *N*-acetylmuramic acid; PP, pyrophosphate; C_{55}, undecaprenyl; TG, transglycosylase; TP, transpeptidase.

10.1021/bi050141j CCC: $30.25
Published on Web 07/29/2005

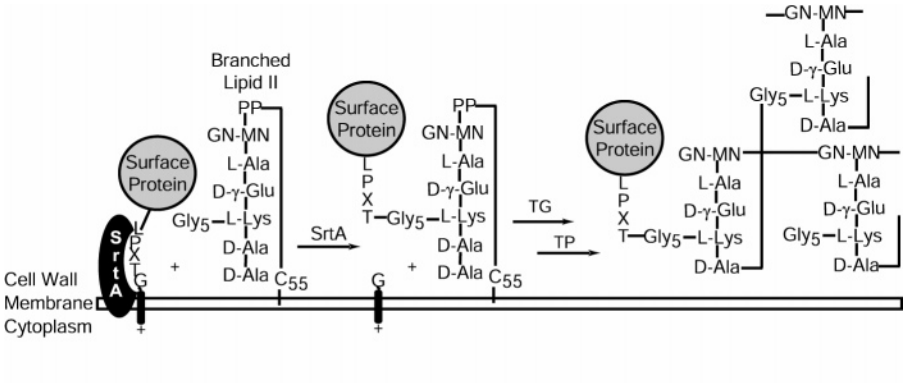

FIGURE 1: SrtA-catalyzed attachment of surface proteins to the peptidoglycan layer of Gram-positive bacteria. SrtA catalyzes surface protein cleavage between the threonine and glycine of a conserved C-terminal LPXTG motif and subsequent amide bond formation between the threonine residue and the pentaglycine branch of the peptidoglycan precursor branched Lipid II. Surface proteins are fully incorporated into mature cross-linked peptidoglycan by the transglycosylase and transpeptidase reactions of late-stage cell-wall biosynthesis.

therapeutics (*14*−*17*), natural plant extracts whose structures are largely undefined (*18*−*20*), and small molecule affinity inactivators that intrinsically lack the ability to specifically target SrtA in vivo (*21*−*23*). These inhibitors have been useful in providing initial mechanistic information with the purified enzyme, for identifying sortase activity within crude cell lysates, and for establishing Cys184 as the active site nucleophile. However, it has become apparent that a more in-depth understanding regarding the kinetic and catalytic mechanism of the SrtA-catalyzed reaction will be necessary for the development of potent and selective SrtA inhibitors with in vivo efficacy. Specifically, knowledge regarding the kinetic and chemical mechanisms will ultimately enable the design of mechanism-based inhibitors or those that mimic elements of the transition state.

Understanding the molecular basis of SrtA catalysis has been complicated by the recent development of several conflicting mechanistic models, rendering conclusions about the SrtA catalytic mechanism difficult (*15*, *24*, *25*). These discrepancies arise from differences in active site architecture observed in the NMR and crystal structures determined for *S. aureus* SrtA and for *S. aureus* and *Bacillus anthracis* SrtB and their respective implications for the roles of active site residues His120 and Arg197 in Cys184 activation and catalysis initiation (*24*, *26*−*28*). Drawing definitive conclusions to describe the true nature of the SrtA catalytic mechanism requires a more detailed analysis of the specific roles played by SrtA active site residues.

Analysis of the SrtA kinetic mechanism will provide a foundation for establishing the chemical mechanism as well as a framework for inhibitor design for this important class of transpeptidases. In a recent study, employing a fluorescence quenching assay that monitored hydrolysis of an LPXTG-containing peptide by SrtA, Huang et al. tentatively assigned a ping-pong bi-bi kinetic mechanism and determined kinetic parameters for steady-state hydrolysis and transpeptidation (*29*). However, the discovery of complications from inner filter effect quenching in the fluorescence assay resulted in the development of an alternative HPLC-based activity assay and subsequent revision of the steady-state kinetic parameters (*30*). Furthermore, global kinetic analysis of SrtA inhibition by a phosphinate LPXTG peptidomimetic revealed inhibition patterns inconsistent with a simple ping-pong bi-bi kinetic mechanism (*16*).

In this study, we re-evaluate the overall kinetic mechanism of *S. aureus* SrtA and examine aspects of its chemical mechanism. Here we present evidence for a kinetic mechanism for recombinant SrtA in which a kinetically competent hydrolytic shunt pathway is observed. Steady-state and pre-steady-state burst profiles indicate that SrtA acylation is rate-limiting during transpeptidation. To shed light on the nature of the catalytic mechanism employed by SrtA, we performed pH−rate, solvent isotope effect, and proton inventory experiments that collectively suggest a reverse protonation catalytic mechanism which differs from three previously proposed models. These studies lay the groundwork for future studies aimed at defining the specific roles of active site residues in Cys184 activation and transition-state stabilization, ultimately leading to the development of highly potent and selective inhibitors of surface protein anchoring in Gram-positive bacteria.

MATERIALS AND METHODS

Materials. Buffer salts were purchased from Sigma. D_2O was purchased from Aldrich. Standard Fmoc amino acids (Novabiochem), Fmoc-Dap-(Dnp)-OH (Bachem), and NH_2-Gly_5-OH (Bachem) were purchased and used without further purification. Protein purification was performed on a Biocad Sprint chromatography system (Applied Biosystems). Chelating Sepharose fast flow chromatography resin (Pharmacia Biotech) and a HiPrep 26/60 Sephacryl S-200 high-resolution gel filtration column (Pharmacia Biotech) were used according to the manufacturers' recommendations. HPLC was performed using a Thermo Separation Products SpectraSYSTEM equipped with an autosampler and either a semi-preparative Jupiter octadecyl silica column (Phenomenex) or a fast analytical (4.6 mm × 50 mm, 3 μm) octadecyl silica column (Vydac).

Overexpression and Purification of Recombinant SrtA. Recombinant SrtA lacking the 24-amino acid membrane anchor was expressed and purified to homogeneity from *Escherichia coli* BL21(DE3) cells harboring the pET15b-$SrtA_{\Delta 24}$ plasmid (*31*). Briefly, cells were grown in Luria broth at 37 °C with 100 μg/mL ampicillin to an OD_{580} of 0.8. IPTG (1 mM) was added to induce expression of SrtA, and cells were harvested after 3 h. Cells were resuspended in 150 mM NaCl, 50 mM Tris, 5 mM imidazole, and 10% glycerol (pH 7.5) and lysed using an EmulsiFlex-C5 high-pressure ho-

mogenizer (Avestin, Inc.). The resultant lysate was clarified by centrifugation and applied to a chelating Sepharose fast flow column. SrtA was eluted with a linear gradient from 5 to 500 mM imidazole over the course of 1 h. Fractions containing SrtA were pooled, concentrated, and loaded onto a HiPrep 26/60 Sephacryl S-200 gel filtration column previously equilibrated with 150 mM NaCl, 50 mM Tris, 5 mM $CaCl_2$, 0.1% β-mercaptoethanol, and 10% glycerol (pH 7.5). Pure SrtA fractions were concentrated to 100 μM using an Amicon stirred cell concentrator (Millipore). The SrtA concentration was determined using a calculated extinction coefficient ($\epsilon_{280} = 17\,420\ M^{-1}\ cm^{-1}$).

Solid-Phase Synthesis of Sortase Substrates. Peptide substrates for sortase activity assays were synthesized by the Fmoc/piperidine solid-phase strategy with PAL resin on a 0.25 mmol scale using an Applied Biosystems 433A synthesizer. Peptides were cleaved using a TFA/water mixture (95:5) for 3 h. Excess TFA was removed by rotary evaporation, and the peptides were precipitated using cold diethyl ether, filtered with a fine porosity fritted glass filter, dissolved in water, and lyophilized to afford the desired crude peptide products. All peptides were purified by HPLC using a semipreparative C_{18} Jupiter column to ≥98% purity and analyzed by MALDI-TOF MS. Purified peptides were lyophilized and stored desiccated at −20 °C.

HPLC Assay for Sortase Activity. Sortase activity was monitored as described previously (*30*) in buffer R [150 mM NaCl, 5 mM $CaCl_2$, and 300 mM Tris-HCl (pH 7.5)] with NH_2-Gly_5-OH (2 mM), SrtA (1 μM), and varying concentrations of Abz-LPETG-Dap(Dnp)-NH_2 (from 0 to 18.4 mM).

Bisubstrate Steady-State Kinetic Analysis. Bisubstrate kinetic analysis was performed at Abz-LPETG-Dap(Dnp)-NH_2 concentrations from 1 to 10 mM and NH_2-Gly_5-OH concentrations from 50 to 1000 μM with 100 nM SrtA. Activity was assayed using the HPLC-based method. The data were fit to a ping-pong bi-bi mechanism (eq 1), and a ping-pong bi-bi partial hydrolytic shunt mechanism (eq 2) using the GraFit global fitting program (Erithacus Software). Derivations of steady-state rate equations for each kinetic model were performed using the methods outlined by Segel (*32*) and the program REFERASS (*33*). For simplicity, the hydrolytic shunt was assumed to be irreversible and first-order, an approach previously validated with γ-glutamyl transpeptidase (*34*),

$$v_p = \frac{k_{cat}[E_0][A][B]}{K_{mb}[A] + K_{ma}[B] + [A][B]} \quad (1)$$

$$v_p = \frac{k_{cat\_h}[E_0]K_{mb}[A] + k_{cat\_t}[E_0][A][B]}{K_{ia}K_{mb} + K_{mb}[A] + K_{ma}[B] + [A][B]} \quad (2)$$

where v_p is the velocity of the formation of NH_2-G-Dap-(Dnp)-NH_2, k_{cat_h} is the overall rate constant for the hydrolytic reaction, k_{cat_t} is the overall rate constant for the transpeptidation reaction, $[E_0]$ is the enzyme concentration, [A] is the concentration of Abz-LPETG-Dap(Dnp)-NH_2, [B] is the concentration of NH_2-Gly_5-OH, K_{ma} is the K_m for Abz-LPETG-Dap(Dnp)-NH_2, K_{mb} is the K_m for NH_2-Gly_5-OH, and K_{ia} is the inhibition constant for Abz-LPETG-Dap(Dnp) as a product inhibitor. Equation 2 is a modified form of eq 1, describing a ping-pong bi-bi reaction with a competing second substrate (H_2O) and the formation of a unique second product (the LPXT-containing peptide acid) (*32*, *34*). The goodness of fit was measured by reduced χ^2 analysis.

Analysis of Steady-State Burst Kinetics. SrtA activity was assayed as described above using 1 mM Abz-LPETG-Dap-(Dnp)-NH_2 at enzyme concentrations of 1, 1.5, and 2 μM in the presence or absence of 2 mM NH_2-Gly_5-OH. Product formation was monitored in 20 s intervals from 60 to 200 s. Resulting plots were analyzed by linear regression analysis.

Pre-Steady-State Kinetic Analysis. Pre-steady-state kinetic analysis was performed with a Biologic rapid quench flow apparatus. For added sensitivity in quantifying reaction products, the alternate substrate Dap(Dnp)-LPETG-K(Abz) was employed. Reactions were initially carried out in both the absence and presence of the NH_2-Gly_5-OH nucleophile. Preliminary results indicated that the reactions that did not include NH_2-Gly_5-OH were biphasic, whereas reactions that included NH_2-Gly_5-OH were monophasic; therefore, all subsequent experiments were performed in the absence of NH_2-Gly_5-OH. SrtA (100 μM in 2× buffer R) was loaded into syringe 1; Dap(Dnp)-LPETG-K(Abz) (5 mM) was loaded into syringe 2, and 1 N HCl was loaded into syringe 3. Assays were performed at 37 °C using an externally controlled circulating water bath. Reactions were initiated by rapid mixing of equal volumes of syringe 1 and syringe 2, and were quenched by rapid mixing with an equal volume of syringe 3. Samples at time points between 50 ms and 1 s were collected in continuous mode by altering both the volume of the delay loops and the flow rate. Time points between 2 and 4 s were assessed in delay mode where the reaction mixture was allowed to age for the indicated time before being quenched and expelled. Time points of 10 s or longer were quenched manually. Quenched reaction mixtures were analyzed by HPLC, and the presence of the G-K(Abz) product was detected by fluorescence ($\lambda_{ex} = 317$ nm, $\lambda_{em} = 420$ nm) and quantified by peak integration. Using GraFit (Erithacus Software), data were fit to eq 3 which describes an exponential burst phase followed by a linear steady-state phase of product formation,

$$P_t = \frac{k_{acyl\_obs}k_{hydr\_obs}[E]t}{k_{acyl\_obs} + k_{hydr\_obs}} + \frac{(k_{acyl\_obs})^2[E][1 - e^{-(k_{acyl\_obs}+k_{hydr\_obs})t}]}{(k_{acyl\_obs} + k_{hydr\_obs})^2} \quad (3)$$

where P_t is the amount of product formed after time t, k_{acyl_obs} is the observed rate constant for the formation of the acyl−enzyme intermediate, and k_{hydr_obs} is the observed rate constant for the hydrolysis of the acyl−enzyme intermediate.

High-Resolution Fourier-Transform MS/MS Analysis of Sortase Reaction Intermediates. SrtA (1 μM) was mixed with Abz-LPETG-Dap(Dnp)-NH_2 (1 mM) under standard reaction conditions, concentrated at pH 4, and desalted by passage over a Vydac C_4 column. Protein mixtures were introduced by microelectrospray at 1 μL/min into 50 μm inside diameter fused silica tapered to a conical tip (New Objective, Cambridge, MA) kept at 2.2 kV above the FTMS inlet voltage. Mass spectra were recorded on a custom 8.5 T quadrupole Fourier-transform ion cyclotron resonance (Q-FTICR) mass spectrometer, described in detail elsewhere (*35*). Desired ions were isolated using a multichannel stored

waveform inverse Fourier-transform (SWIFT; 5 *m*/*z* window per notch) (*36*) and fragmented using infrared multiphoton dissociation (IRMPD) (*37*) for 120 ms at 80% power. Transients were zero-filled once, and a Hamming apodization was applied prior to the Fourier-transform of the transient. The IRMPD spectra were processed using the THRASH algorithm (*38*), and the resulting fragment lists were then analyzed in the ProSight PTM environment (*39*).

Determination of pH Stability of SrtA. To determine the pH stability of SrtA, 10 μM enzyme was preincubated in buffer A (50 mM acetic acid, 50 mM MES, 100 mM Tris, 5 mM $CaCl_2$, and 150 mM NaCl) adjusted to pH 3.55−7.5 or buffer B (50 mM MES, 100 mM Tris, 50 mM CAPS, 5 mM $CaCl_2$, and 150 mM NaCl) adjusted to pH 5.5−11.0, at 37 °C for 30 min. SrtA activity was then assayed in duplicate with 1 μM SrtA and 0.26 mM Abz-LPETG-Dap(Dnp)-NH_2 in buffer R at pH 7.5 as described above.

Measurement of the Dependence of k_{cat} and k_{cat}/K_m on pH. Assays were performed in duplicate in buffer A or B with 1 μM SrtA and the indicated concentration of Abz-LPETG-Dap(Dnp)-NH_2 as described above. Since saturation of SrtA is difficult to achieve due to substrate solubility, k_{cat} was obtained by measuring the rate of product formation at the highest achievable concentration of Abz-LPETG-Dap(Dnp)-NH_2 (15.6 mM), and k_{cat}/K_m was calculated by dividing v, the initial velocity obtained at substrate concentrations well below K_m, by the Abz-LPETG-Dap(Dnp)-NH_2 concentration (0.26 mM) and normalizing for the amount of SrtA present (1 μM) (*30*). The data were modeled using GraFit (Erithacus). Profiles obtained for k_{cat} and k_{cat}/K_m were fit to eq 4, describing a bell-shaped function with two associated pK_a values,

$$\log y_{obs} = \log\left(\frac{y_{max}}{1 + [H^+]/K_{a1} + K_{a2}/[H^+]}\right) \qquad (4)$$

where pK_1 and pK_2 represent the pK_a values of catalytically competent functional groups and y_{max} is the pH-independent value of k_{cat} or k_{cat}/K_m.

Solvent Isotope Effects. To determine the effect of heavy water on kinetic parameters K_m, k_{cat}, and k_{cat}/K_m, we employed the HPLC assay described above. Reaction mixtures contained 99% D_2O, and the concentration of Abz-LPETG-Dap(Dnp)-NH_2 was varied from 0.05 to 19.2 mM. SrtA substrates were dissolved in D_2O prior to addition. Buffer R, described above, was prepared in H_2O, lyophilized to dryness, redissolved in an equivalent volume of D_2O, and adjusted with DCl or NaOD to the appropriate pH meter value (where the pD equals the pH reading + 0.4). Kinetic parameters were obtained by fitting the data to the Michaelis−Menten equation using SigmaPlot (SYSTAT Software Inc.), and solvent isotope effects were calculated as the ratio of values obtained in H_2O to those in 99% D_2O.

Proton Inventory Measurements. Assays were performed as described above in standard buffer (pL 7.5) with different deuterium atom fractions n (from 0 to 0.99) achieved by combining appropriate volumes of H_2O and D_2O buffers. Results were fit using linear regression analysis.

pH Dependence of SrtA Inactivation by Iodoacetamide. Assays were performed in the presence of 0.06−7 mM iodoacetamide with 0.26 mM Abz-LPETG-Dap(Dnp)-NH_2 over a pH range of 7.0−10.0 using buffers A and B described above. Product formation as a function of time was monitored using the HPLC-based activity assay. The first-order inactivation rate constant (k_{obs}) was obtained by fitting the resulting progress curves to a single-exponential function. The variation of k_{obs} with iodoacetamide concentration was used to calculate a second-order rate constant for inactivation (k_{inact}) as described by Kitz and Wilson (*40*). The pH dependence of k_{inact} was fit to eq 5 to obtain an estimate of the pK_a. Equation 5 describes a single ionization with a midpoint of K_a,

$$\log y = \log\left(\frac{y_{min} + y_{max}\dfrac{K_a}{[H^+]}}{1 + \dfrac{K_a}{[H^+]}}\right) \qquad (5)$$

where y_{min} and y_{max} are the minimum value of k_{inact} at low pH and the maximum value of k_{inact} at high pH, respectively.

RESULTS AND DISCUSSION

Bisubstrate Steady-State Kinetic Analysis. Previously, the kinetic mechanism of SrtA transpeptidation was tentatively described as ping-pong bi-bi (*29*). However, recombinant SrtA has been shown to catalyze the hydrolysis of peptides containing the LPXTG motif in vitro in the absence of external nucleophiles (*41*); therefore, another factor to consider is whether the SrtA-catalyzed proteolysis reaction occurs at a rate that is sufficiently high to complicate standard kinetic schemes. To address this issue and to evaluate the kinetic parameters of SrtA transpeptidation in the context of our HPLC-based assay, we performed a series of bisubstrate kinetic experiments in which the initial velocity of SrtA-catalyzed transpeptidation was measured while simultaneously varying the concentrations of Abz-LPETG-Dap(Dnp)-NH_2 and NH_2-Gly_5-OH substrates.

Bisubstrate kinetic experiments resulted in the family of lines shown in Figure 2. The Lineweaver−Burk plot obtained by varying NH_2-Gly_5-OH at fixed concentrations of Abz-LPETG-Dap(Dnp)-NH_2 resulted in a family of curved lines characteristic of a mechanism incorporating a hydrolytic shunt (*34*). The initial velocity patterns were globally fit to the two kinetic models described by eqs 1 and 2 for ping-pong bi-bi and ping-pong bi-bi hydrolytic shunt mechanisms (Figure 3), with χ^2 analysis yielding values of 0.000681 and 0.000495, respectively. As anticipated, the significance of the differences in reduced χ^2, as measured by F-test analysis, indicates that the kinetic model incorporating the hydrolytic shunt fits the data significantly better than a simple ping-pong kinetic model. Furthermore, kinetic parameters determined from fitting to eq 2 were as follows: $k_{cat\_t} = 0.28 \pm 0.02$ s^{-1}, $k_{cat\_h} = 0.086 \pm 0.015$ s^{-1}, $K_{ma} = 7.33 \pm 1.01$ mM, $K_{mb} = 196 \pm 64$ μM, and $K_{ia} = 3.39 \pm 0.95$ μM. These kinetic parameters are in excellent agreement with k_{cat}^{app} and k_{cat}/K_{ma}^{app} values previously reported by Kruger and coworkers (*30*). Such a kinetic mechanism has been observed for related enzymes, including γ-glutamyl transpeptidase, transglutaminase, and glucose 6-phosphatase (*34*, *42*, *43*). Previously reported nonlinear SrtA inhibition profiles obtained with the competitive phosphinic peptidomimetic

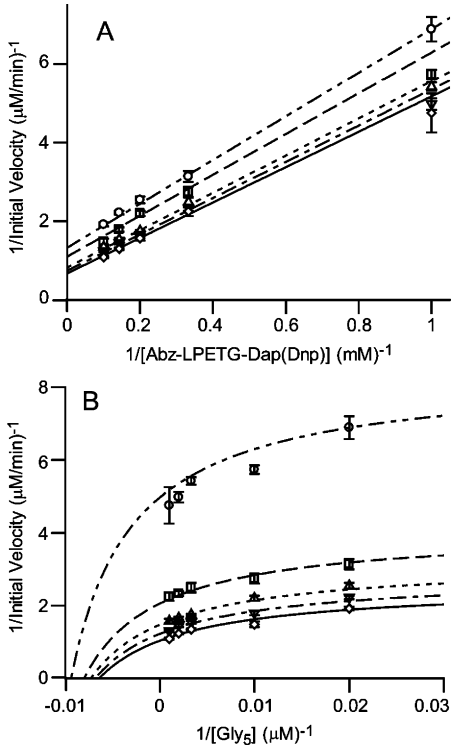

FIGURE 2: Bisubstrate kinetic analysis of SrtA transpeptidation. The concentrations of Abz-LPETG-Dap(Dnp) and Gly_5 were simultaneously varied in the HPLC-based SrtA activity assay. Each data point is the average of three independent measurements, and the lines through the points were obtained by global fitting of the data to eq 2 using GraFit. (A) Double-reciprocal plot of initial velocity vs Abz-LPETG-Dap(Dnp) concentration at five fixed Gly_5 concentrations: 50 (○), 100 (□), 300 (△), 500 (▽), and 1000 μM (◇). (B) Double-reciprocal plot of initial velocity vs Gly_5 concentration at five fixed Abz-LPETG-Dap(Dnp) concentrations: 1 (○), 3 (□), 5 (△), 7 (▽), and 10 mM (◇).

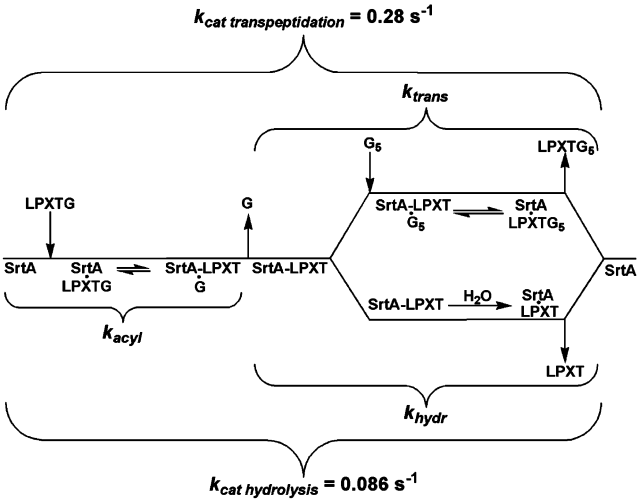

FIGURE 3: Ping-pong hydrolytic shunt kinetic scheme depicting potential rate-limiting steps. SrtA catalyzes the cleavage of the LPXTG-containing substrate with acylation of Cys184 and release of the C-terminal portion of the protein. Next, the peptidoglycan nucleophile (G5) attacks the acylated enzyme to form a transpeptidation product with regeneration of free SrtA. In an alternate hydrolytic shunt pathway, water may serve as the incoming nucleophile to release a hydrolysis product. Acylation is rate-limiting in the transpeptidation reaction, whereas deacylation is rate-limiting in the hydrolytic shunt.

inhibitor NH_2-YALPE-AlaΨ{PO_2H-CH_2}Gly-EE-NH_2 also support the existence of a kinetically competent hydrolytic shunt (*16*).

In a ping-pong mechanism with a partial hydrolytic shunt, there are three potentially rate-limiting chemical steps: the generation of the acyl−enzyme intermediate (k_{acyl}), the hydrolysis of the acyl−enzyme intermediate (k_{hydr}), and the formation of the transpeptidation product through attack of Gly_5 on the acyl−enzyme intermediate (k_{trans}) as shown in Figure 3. By comparing the values of k_{cat_h} and k_{cat_t} extracted from fitting bisubstrate kinetic data to eq 2, we were able to gain insight into whether the first or second half of the overall hydrolysis and transpeptidation reactions is rate-limiting. Since both the hydrolysis and transpeptidation reactions are governed by the same k_{acyl}, if k_{acyl} was rate-limiting overall, then k_{cat_h} would equal k_{cat_t} (Figure 3). However, the hydrolysis reaction is significantly slower ($k_{cat\_h} = 0.086\ s^{-1}$) than the transpeptidation reaction ($k_{cat\_t} = 0.28\ s^{-1}$), indicating that k_{hydr} is less than k_{acyl} and that the rate-limiting step in the hydrolysis reaction occurs after the release of the first product. In contrast, for the transpeptidation reaction, it is surmised that k_{cat_t} must be less than or equal to k_{acyl}.

Steady-State and Pre-Steady-State Burst Kinetics. In ping-pong kinetics, if the rate constant of the second step (k_{trans} or k_{hydr}) is much slower than the first (k_{acyl}), a burst in the formation of the first product, with an amplitude equal to the enzyme concentration, is expected (*44*). Since comparison of k_{cat_h} and k_{cat_t} allowed us to infer that k_{hydr} is less than k_{acyl}, we anticipated burst kinetics for the hydrolysis reaction; however, the analysis described above did not permit us to draw conclusions regarding the relative magnitude of k_{acyl} and k_{trans} in the transpeptidation reaction. Therefore, to analyze the relative rates of these processes, we looked for the occurrence of a burst phase in steady-state experiments both in the absence (hydrolysis) and in the presence (transpeptidation) of Gly_5.

SrtA activity, with and without Gly_5, was monitored at three enzyme concentrations (1, 1.5, and 2 μM) over 200 s as shown in Figure 4A. The amount of product formed in assays containing Gly_5 extrapolates back to zero, demonstrating the lack of a burst phase. As expected, the amount of product formed in the absence of Gly_5 extrapolates back to the positive *y*-axis, at a value closely approximating the concentration of SrtA in the assay (1 μM SrtA = 1.1 μM product, 1.5 μM SrtA = 1.5 μM product, and 2 μM SrtA = 2.1 μM product), signifying the presence of a burst phase (Figure 4A,B). To verify these findings, we performed rapid-quenching experiments to directly examine the kinetics of pre-steady-state turnover.

Using a rapid quench flow apparatus in combination with manual quenching, reactions were assayed over a time range from 0.05 to 100 s. To increase the sensitivity of the existing HPLC assay, we reversed the orientation of the chromophores on the Abz-LPETG-Dap(Dnp) substrate and synthesized Dap(Dnp)-LPETGK(Abz), enabling us to monitor the formation of GK(Abz) by fluorescence. We confirmed that the kinetic parameters for Dap(Dnp)-LPETGK(Abz) were identical to those for Abz-LPETG-Dap(Dnp) (data not shown). Since saturating concentrations of Dap(Dnp)-LPETGK(Abz) were not achievable, we performed assays at 2.5 mM ($\sim 0.33K_m$) Dap(Dnp)-LPETGK(Abz) while the concentration of Gly_5 was saturating (2 mM).

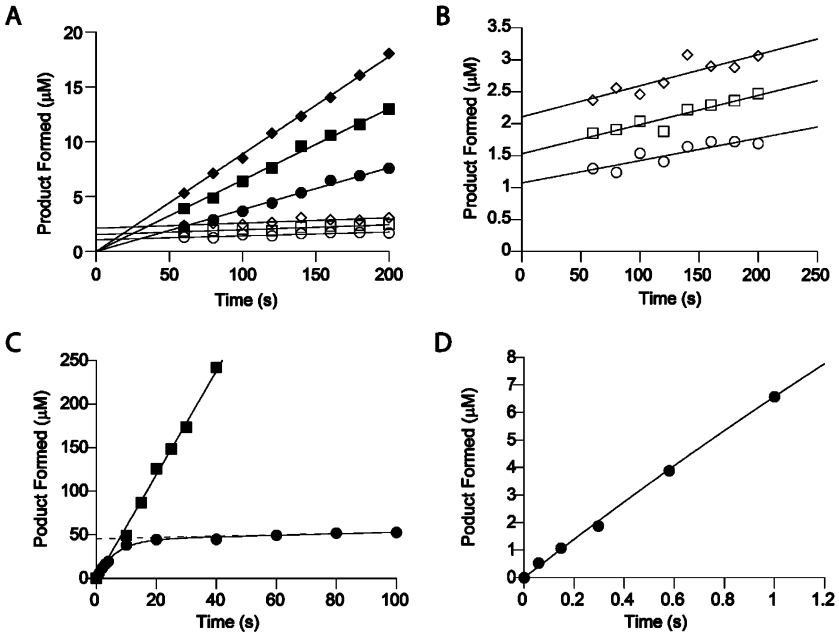

FIGURE 4: Steady-state and pre-steady-state burst kinetics. (A) Steady-state analysis of SrtA activity demonstrating a burst only in the absence of the Gly_5 nucleophile. Empty symbols indicate the absence of Gly_5. Filled symbols indicate the presence of Gly_5 (2 mM). SrtA concentrations are as follows: 1 (○ and ●), 1.5 (□ and ■), and 2 μM (◇ and ◆). The solid lines through the data were generated using linear regression analysis. (B) Expanded view of data obtained in the absence of Gly_5 showing positive *y*-intercepts approximately equal to SrtA concentration. (C) Pre-steady-state analysis of SrtA activity in the presence of 2 mM Gly_5 (■) or in the absence of Gly_5 (●). The solid lines through the data were obtained from linear regression analysis for data obtained in the presence of Gly_5, and from fitting to eq 3 for data recorded in the absence of Gly_5. The dotted line was generated from linear regression analysis of the steady-state portion of the curve obtained in the absence of Gly_5. (D) An expanded view of early time points analyzed in the absence of Gly_5 shows that the curve passes through the origin.

As shown in Figure 4C, there was a linear dependence on the formation of product as a function of time in the presence of Gly_5, indicating the lack of a burst phase as predicted. In the absence of Gly_5, a distinctive burst phase followed by a steady-state rate of product formation was observed (Figure 4C,D). Nonlinear fitting of these data to eq 3 produced estimates of 0.16 s^{-1} for k_{acyl_obs} and 0.002 s^{-1} for k_{hydr_obs}. Since this experiment could not be performed at saturating substrate concentrations, the observed rate constants are likely smaller than they would be at saturating substrate concentrations.

The observation of burst kinetics in the hydrolysis reaction but not in the transpeptidation reaction (Figure 4) suggests that the identity of the rate-limiting step is different in the competing hydrolysis and transpeptidation reactions. The burst of product formation in the hydrolysis reaction suggests that steps *after* the release of the first product are rate-limiting, and that k_{cat_h} reflects k_{hydr}. In contrast, the lack of a burst in the transpeptidation reaction suggests that steps prior to the release of the first product are rate-limiting, and that k_{cat_t} reflects k_{acyl}. Despite arriving at a different conclusion regarding the overall kinetic mechanism of SrtA, Huang and co-workers also observed that hydrolysis of the acyl−enzyme intermediate is rate-limiting in the hydrolysis reaction, whereas acylation is rate-limiting in the transpeptidation reaction (*29*).

High-Resolution Fourier-Transform MS/MS Analysis of Sortase Reaction Covalent Intermediates. Although the kinetic evidence is consistent with the formation of an acyl−enzyme intermediate, similar burst kinetics might be observed in the absence of a covalent intermediate if the rate-limiting step of the reaction is the release of the second product instead of the second chemical step (*44*). To verify that SrtA proceeds through an acyl−enzyme intermediate, we performed Fourier-transform MS/MS on $SrtA_{\Delta N24}$ before and after reaction with Abz-LPETG-Dap(Dnp).

The mass of unmodified SrtA was observed to be 21 146.8 Da (21 147.8 Da theoretical value, data not shown). After reaction with with Abz-LPETG-Dap(Dnp), a mass increase of 559.5 Da was observed, consistent with the modification of SrtA by Abz-LPET (Figure 5). To localize the site of enzyme modification, the modified SrtA species was analyzed by ESI FT-MS/MS using IRMPD fragmentation. Figure 5 shows the spectra of the modified enzyme and observed *b*- and *y*-ion fragmentation positions. While the exact location of the modification could not be determined precisely given the pattern of fragment ions, the covalent modification has been localized to the section of SrtA between Ser116 and Asp186. This region contains Cys184 which has been demonstrated to be functionally important through structural (*24*, *26*), affinity labeling (*14*, *15*, *21*), and mutational analyses (*25*). These mass spectrometry results confirm a covalent intermediate and, when taken together with the results from steady-state bisubstrate kinetic analyses and pre-steady-state kinetic studies, provide support for a ping-pong bi-bi hydrolytic shunt kinetic mechanism for recombinant SrtA.

pH Dependence of SrtA-Catalyzed Transpeptidation. To identify catalytically important ionizations and to gain insight into the mechanism of SrtA-catalyzed transpeptidation, we measured kinetic parameters k_{cat} and k_{cat}/K_m as a function of pH over the pH range from 3.5 to 11.0. Because of solubility limitations at low pH, k_{cat} was only observable in the pH range from 5.5 to 11.0, whereas data for k_{cat}/K_m were obtained

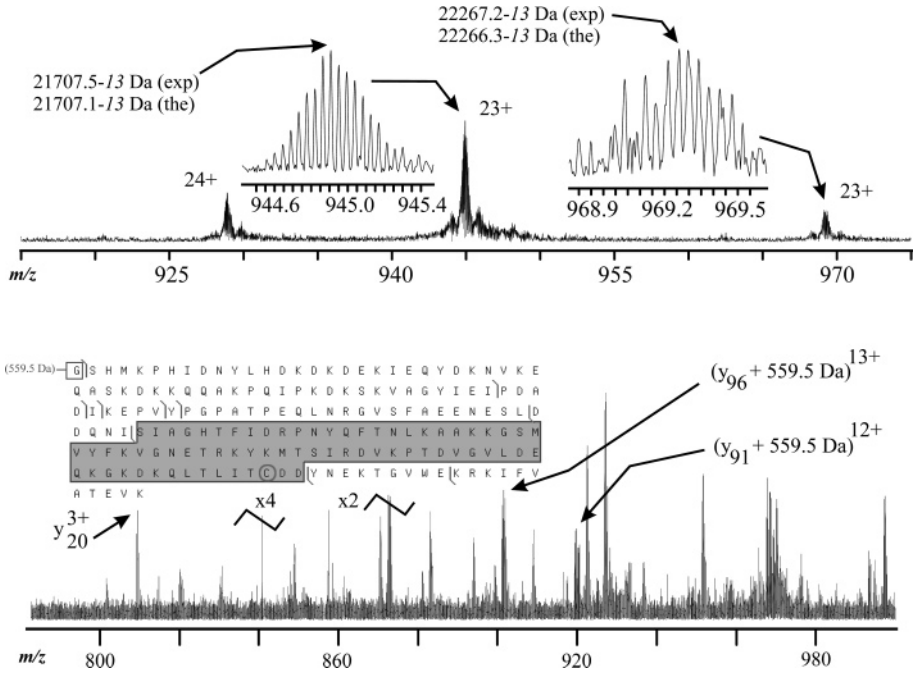

FIGURE 5: Fourier-transform MS/MS localization of a SrtA covalent intermediate produced during catalysis. The top panel shows ESI-FTMS spectra (+23 and +24 charge states) of the SrtA enzyme treated with Abz-LPETGDap(Dnp) showing a 559.5 Da increase in mass due to formation of an Abz-LPET-SrtA covalent adduct. The mass of the unmodified enzyme was determined experimentally to be 21 146.8 Da (21 147.8 Da theoretical value). The bottom panel shows the primary sequence of SrtA and the ESI-FT MS/MS IRMPD spectrum of the enzyme−substrate adduct. The Abz-LPET-SrtA adduct is localized to the Ser116−Asp186 fragment (gray) that contains Cys184 (circled C in last shaded row), the active site nucleophile. Although the molecular mass of this enzyme−adduct complex is consistent with the formation of a thioester intermediate, it is not confirmatory given the large size of the fragment ions generated by IRMPD fragmentation during MS/MS.

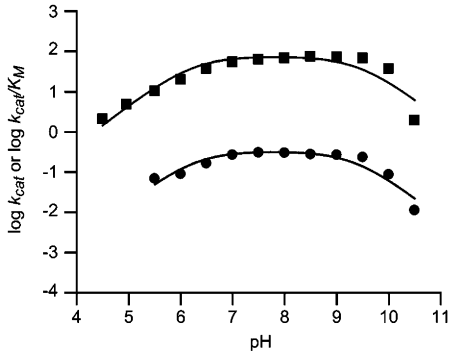

	pK_1	pK_2
k_{cat}	6.3 ± 0.2	9.4 ± 0.2
k_{cat}/K_m	6.2 ± 0.2	9.4 ± 0.2

FIGURE 6: pH dependence of SrtA catalysis. The log of k_{cat} (●) and the log of k_{cat}/K_M (■) for the SrtA-catalyzed transpeptidation reaction are plotted as a function of pH. Each point is the average of two measurements. The solid lines through the points were obtained by fitting the data to eq 4.

at a pH as low as 3.5. SrtA was found to be stable over the entire pH range that was tested (data not shown). Bell-shaped profiles were obtained for both k_{cat} and k_{cat}/K_m as shown in Figure 6. Fitting the data to eq 4 yielded pK_a values of 6.3 ± 0.2 and 9.4 ± 0.2 with a pH-independent value of 0.33 ± 0.07 s^{-1} for k_{cat} ($\chi^2 = 0.027$), implicating the involvement of two titratable groups of the enzyme−substrate complex in the conversion of substrate to product. Likewise, pK_a values of 6.2 ± 0.2 and 9.4 ± 0.2 for k_{cat}/K_m, with a pH-independent value of 75 ± 2 M^{-1} s^{-1} ($\chi^2 = 0.055$), indicate that the titratable groups are localized to the free enzyme and participate in substrate to product conversion. Since, the pK_a values determined for k_{cat} and for k_{cat}/K_m are nearly identical, we may also infer that the binding of the Abz-LPETG-Dap(Dnp) substrate to SrtA does not significantly affect the pK_a of catalytically important SrtA active site residues (*45*).

Table 1: Solvent Isotope Effects on SrtA Kinetic Parameters

	k_{cat} (s^{-1})	K_M (mM)	k_{cat}/K_M (M^{-1} s^{-1})
H_2O	0.48 ± 0.004	6.4 ± 0.1	75 ± 2
D_2O	0.54 ± 0.006	4.1 ± 0.1	132 ± 5
H_2O/D_2O	0.89 ± 0.01	1.6 ± 0.1	0.57 ± 0.03

Although it is not yet possible to definitively assign the observed ionizations to specific amino acid side chains in SrtA, the pK_a values observed in this study are highly consistent with the values of 6.6−7.0 measured for His120 from NMR titrations, and the value of 9.4 estimated for Cys184 from the pH dependence of SrtA inactivation by the peptidyl vinyl sulfone Cbz-Leu-Pro-Ala-Thr-SO_2Ph (*15*). Of note as well, the observed ionizations for SrtA are less consistent with the assigned ionizations of the cysteine hydrolase papain that utilizes an imidazolium−thiolate ion pair thiol activation mechanism and manifests pK_a values of 3.3 (Cys thiolate) and 8.5 (His imidazolium) (*46*, *47*). They do, however, correlate with the values of 6.2 (His) and 8.5 (Cys) observed for the cysteine hydrolase picornain 3C (*48*).

Solvent Isotope Effects on SrtA-Catalyzed Transpeptidation. To identify the nature of the rate-limiting step in the acylation half of the SrtA-catalyzed transpeptidation reaction, kinetic parameters k_{cat} and K_m were measured in H_2O and in 99% D_2O (Table 1). The measured parameters revealed an increase in the SrtA reaction rate in D_2O, or an inverse

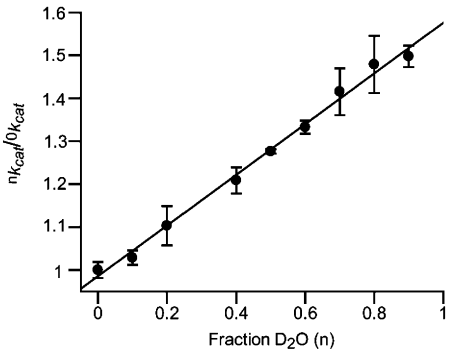

FIGURE 7: Proton inventory on k_{cat}. The ratio of k_{cat} measured in the fraction (n) of D_2O to that measured in 100% H_2O is plotted as a function of the mole fraction of D_2O in the reaction. Data were collected at pH 7.5 in the pH-independent region of the SrtA pH−activity profile. Each point is the average of two measurements. The solid line through the data is a line of best fit obtained using linear regression analysis.

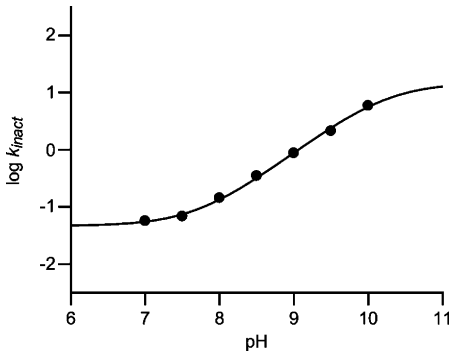

FIGURE 8: pH dependence of SrtA inactivation by iodoacetamide. The log of k_{inact}, the second-order rate constant for alkylation of SrtA with iodoacetamide, is plotted as a function of pH. The solid line through the points was generated by fitting the data to eq 5, yielding a pK_a of 10.2 ± 0.1 with a y_{min} of 0.046 ± 0.004 M^{-1} s^{-1} and a y_{max} of 14.8 ± 4.3 M^{-1} s^{-1}.

isotope effect. As indicated in Table 1, a minor effect on k_{cat} was observed ($^{D_2O}k_{cat} = 0.89$), and the K_m of SrtA for Abz-LPETG-Dap(Dnp) decreased from 6.4 to 4.1 mM in D_2O ($^{D_2O}K_m = 1.6$). These effects combined correspond to a 1.8-fold increase in SrtA catalytic efficiency in D_2O ($^{D_2O}k_{cat}/K_m = 0.57$). Since the sulfhydryl group has an inverse fractionation factor, we believe that the inverse nature of the observed isotope effect can be attributed to Cys184 (*49*, *50*). Further consideration, as discussed below, led us to interpret this inverse SIE as an equilibrium effect on the interconversion of thiol and thiolate forms of Cys184.

In an effort to confirm the number of hydrogenic sites implicated in the rate-limiting transition state of SrtA catalysis, we performed a proton inventory. The parameter k_{cat} was measured as a function of the fraction of D_2O in the reaction (0−99%). The resulting plot was linear ($r^2 = 0.997$), suggesting the involvement of a single hydrogenic site in the isotope-sensitive step of substrate to product conversion (Figure 7) (*49*).

pH Dependence of SrtA Inactivation by Iodoacetamide. To assess whether the resting state of Cys184 is a thiol or a thiolate, we examined the pH dependence of SrtA inactivation by iodoacetamide. Iodoacetamide possesses much greater reactivity with the thiolate form of cysteine as compared to the free thiol (*51*). A plot of k_{inact} as a function of pH is shown in Figure 8. Fitting the data to eq 5 afforded a pK_a of 10.2 ± 0.1 with a y_{min} of 0.046 ± 0.004 M^{-1} s^{-1} and a y_{max} of 14.8 ± 4.3 M^{-1} s^{-1}. It is important to note that the calculated pK_a for this titration falls just outside the pH range in which data was collected (pH 7−10) and thus may not accurately reflect the true pK_a of Cys184. However, this result is not inconsistent with the earlier calculations of a pK_a of 9.4 for the basic limb of SrtA pH−rate profiles.

Surprisingly, the pH dependence of SrtA alkylation is sigmoidal rather than biphasic, as has been observed for both papain, which utilizes an ion pair mechanism, and picornain 3C, which is thought to employ a general base mechanism (*48*). The profiles for alkylation of papain and picornain 3C by iodoacetamide are characterized by two ionizations with a sigmoidal contribution from free thiolate at high pH (greater than ~8) and a bell-shaped contribution at lower pH (less than ~8) which is attributed to the reaction of the cysteine thiolate or thiol mediated by the histidine imidazolium or imidazole, respectively (*48*, *51*). In both cases, the pK_a's of the titrations observed in the pH dependence of iodoacetamide inactivation correlate with the pK_a's observed in the corresponding bell-shaped pH−activity profiles. The sigmoidal curve observed for SrtA inactivation by iodoacetamide, therefore, not only infers a lack of significant thiolate concentrations in the pH range of maximal sortase activity (pH 7−9) but also suggests that there is no measurable contribution from a second ionizable residue, such as His120 or Arg197, in mediating the reactivity of Cys184. On the basis of this result, we infer that SrtA possesses a distribution of catalytically important ionized residues different from those of both papain and picornain 3C, and that its mechanism may also differ significantly from the ion pair mechanism observed for papain and from the general base mechanism implicated for picornain 3C.

Previous Models for the Catalytic Mechanism of S. aureus SrtA. As mentioned briefly earlier, structural information for *S. aureus* SrtA, *S. aureus* SrtB, and *B. anthracis* SrtB, combined with preliminary investigations of the *S. aureus* SrtA catalytic mechanism, has led to the development of three conflicting mechanistic models for sortase catalysis (*15*, *24*−*28*). These mechanisms fall into three classes with respect to thiol activation as illustrated in Figure 9.

The first model (Figure 9A) is an ion pair mechanism involving the pairing of Cys184 thiolate with either His120 imidazolium or Arg197 guanidinium ions. In this model, Cys184 is held in an active thiolate form prior to substrate binding and thus does not require activation prior to catalyzing nucleophilic attack on the scissile bond of the peptide substrate. The negatively charged thiolate is balanced by the presence of a positively charged counterion, supplied by the side chains of either His120 or Arg197. Support for this model was first provided by Ilangovan et al., who noted that, in the NMR structure of *S. aureus* SrtA (*24*), His120 and Cys184 share a geometry similar to that observed for papain-like cysteine proteases which have been demonstrated to catalyze proteolysis via a thiolate−imidazolium ion pair thiol activation mechanism (*52*). An ion pair model for SrtA was then fully formulated by Ton-That et al., who used mutational analyses to demonstrate that Cys184 and His120 were required for SrtA catalysis and suggested that these residues were engaged in a thiolate−imidazolium ion pair (*25*). However, ion pair catalysis in papain is characterized

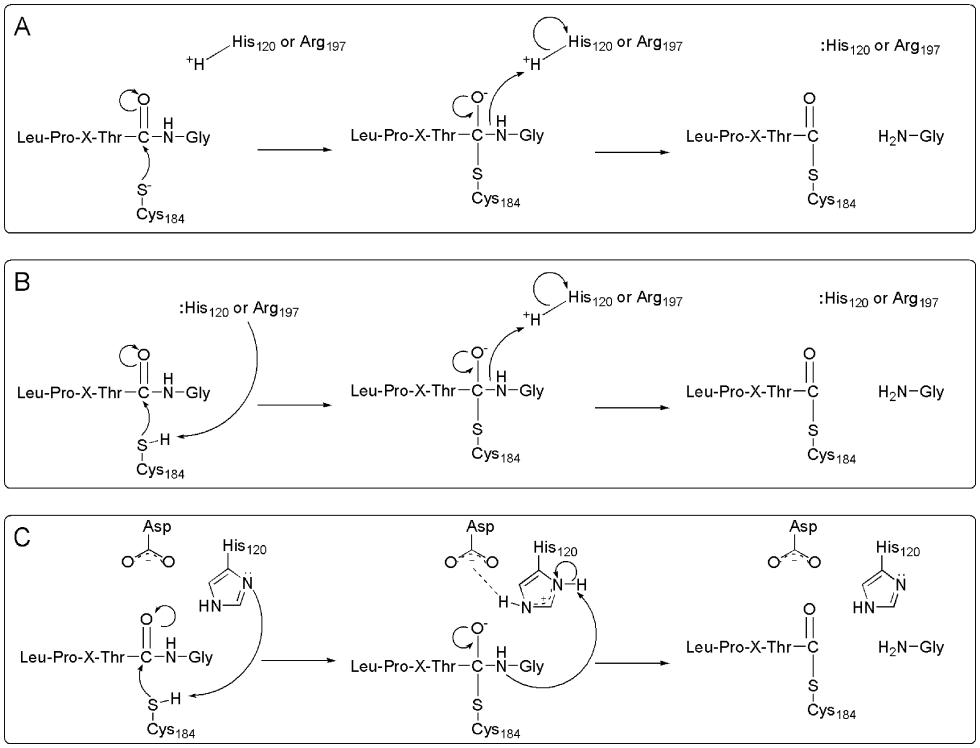

FIGURE 9: Three recently developed mechanistic models for SrtA acylation. The models are based on information obtained from structural studies, as discussed in the text. (A) Thiolate−imidazolium or thiolate−guanidinium ion pair Cys184 thiol activation mechanism. (B) General base activation of Cys184 by His120 or Arg197. (C) Cys-His-Asp catalytic triad activation mechanism with a serine protease-like proton shuttle.

by irregular pK_a's of 3.3 and 8.5 for Cys and His residues, respectively (*46*, *47*), a feature that is inconsistent with the direct measurements of ~9.4 and 7.0 reported by Clubb and co-workers for Cys184 and His120 in SrtA (*15*), respectively, as well as with our own experimental observations (Figure 6).

A variation of this ion pair model was formulated after the involvement of His120 in SrtA catalysis was refuted by Narayana and colleagues who noted a suboptimal interaction distance of 11 Å between the side chain of His120 and the scissile Thr−Gly bond in the crystal structure of SrtA C184A complexed with LPETG peptide (*26*). In the same structure, the conserved side chain of Arg197 was found to be within hydrogen bonding distance of the scissile Thr carbonyl (*26*). This observation, when considered in combination with the similar active site architecture of *S. aureus* SrtB, led to the proposal of a role for Arg197 in Cys184 activation (*27*, *53*).

The second class of mechanistic models for SrtA catalysis is a general base thiol deprotonation activation model in which the identity of the general base is either His120 or Arg197 (Figure 9B). In this model, Cys184 exists in a thiol form in the ground state of the enzyme and requires activation by a general base that abstracts a proton prior to, or concomitantly with, attack on the scissile bond of the substrate. On the basis of the structural observations outlined above, the identity of the general base may be either His120 or Arg197. A similar general base mechanism has been proposed for picornain-like cysteine proteases and is characterized by pK_a values of 6.2 and 8.5 for active site His and Cys residues, respectively (*48*). This type of mechanism was intially proposed for SrtA when Clubb and co-workers (*15*) observed similar pK_a values for His120 and Cys184 of SrtA (see above).

Last, a third general mechanistic model for sortase catalysis involves a Cys-His-Asp catalytic triad (Figure 9C) and is similar to the general base model in that Cys184 requires activation; however, it differs in that an Asp residue would serve to create a proton relay system to facilitate proton abstraction from Cys184 and to stabilize the positive charge on His120 in the transition state. In serine hydrolases, such a serine nucleophile activation mechanism is commonly observed (*54*). This triad thiol activation model model arises from active site structures of the SrtB isoform from *S. aureus* and *B. anthracis* which depict Asp residues within hydrogen bonding distance of the active site His (*28*). Although not previously implicated in catalysis, Asp residues are present at positions 185 and 186 in *S. aureus* SrtA in the vicinity of the active site and thus have the potential to play a role in catalysis. In addition, a growing number of cysteine hydrolases employ a similar Cys-His-Asp catalytic triad thiol activation mechanism, including arylamine *N*-acetyltransferases and bile acid-CoA:amino acid *N*-acyltransferases (*55*, *56*). Interestingly, poliovirus protease 3C is a picornain-like cysteine protease with a Cys-His-Glu catalytic triad (*57*).

In an effort to clarify existing discrepancies in the SrtA literature regarding the involvement of His120 and Arg197 in Cys184 activation, we investigated the pH dependence of SrtA activity. Initial pH activity studies on k_{cat} and on k_{cat}/K_m revealed the presence of two catalytically important ionizations on the free enzyme which are involved in substrate to product conversion (Figure 6). The pK_a values of 6.2 and 9.4 determined from the k_{cat}/K_m profile are consistent with roles for His120 and Cys184 in SrtA catalysis. Accordingly, recent mutational analyses of SrtA support His120 as the source of the pK_a of 6.2 and Cys184 as the residue contributing the higher ionization value of 9.4

(B. A. Frankel and D. G. McCafferty, unpublished observations). Although Marraffini et al. reported that mutation of Arg197 impaired SrtA activity and cited this as evidence for a thiol activation mechanism involving Arg197 (*58*), we did not observe a titration consistent with the expected pK_a of an arginine side chain (12.5). Correspondingly, our recent mutational analyses of Arg197 are more in line with a role for this residue in transition-state stabilization (B. A. Frankel and D. G. McCafferty, unpublished observations).

Criteria for a Holistic Mechanistic Model of SrtA Catalysis. In light of our evaluation of the SrtA kinetic mechanism, solvent deuterium isotope effects, proton inventory, pH−activity profiles, and the reactivity of the active site Cys184 nucleophile by inactivation with iodoacetamide, none of the three aforementioned models for sortase catalysis adequately accounts for all aspects of our experimental observations. Such a holistic mechanistic model should sufficiently (1) account for the low k_{cat} of the SrtA-catalyzed reaction and the high K_m observed for the Abz-LPETG-Dap(Dnp) substrate, as has been observed in this study as well as previously (*30*); (2) provide a justification for the inverse equilibrium solvent isotope effect; (3) explain the involvement of a single exchangeable hydrogenic SrtA site in the rate-limiting step of catalysis, as revealed through proton inventory analysis; (4) provide a basis for the loss of SrtA activity at low and high pH, as observed in the bell-shaped pH−rate profiles; (5) offer consistency with the participation of His120 and Cys184 in SrtA acylation, as implied by the pK_a values measured for catalytically important ionizations that correlate with previously measured pK_a's of His120 and Cys184, and are supported by site-directed mutagenesis of these residues (*15*, *25*); (6) include opposite protonation states for Cys184 and His120 in the ground state of the active form of SrtA, as indicated by the bell-shaped pH−rate profiles; (7) consider the finding that the major population of SrtA will persist with Cys184 in the undissociated thiol form within the pH range of maximal sortase activity, as reflected by the single ionization in the pH dependence of SrtA inactivation with iodoacetamide; and (8) confer an essential role for His120 in SrtA acylation other than modulating the reactivity of Cys184, to be consistent with the lack of participation of His120 in SrtA alkylation with iodoacetamide, while still satisfying criteria 5 and 6.

Our initial interpretation of these findings resulted in the formulation of a mechanistic model for SrtA catalysis, akin to mechanism B in Figure 9, which included the rate-limiting general base activation of Cys184 through proton abstraction by His120. This is analogous to the general base mechanism implicated for picornain 3C (*48*). However, closer inspection of the above criteria suggests that while such a model does satisfy criteria 2, 3, and 5−7, it fails to adequately address criteria 1, 4, and 8. Likewise, re-examination of the two remaining previously proposed sortase mechanisms revealed similar inconsistencies; the Cys-His-Asp catalytic triad model (Figure 9C) is incompatible with criteria 1, 3, 4, and 8, and the ion pair model (Figure 9A) does not account for criteria 1, 7, and 8. Thus, it appears that the catalytic mechanism of SrtA differs from all three of the previously proposed models.

A Reverse Protonation Model for SrtA Catalysis. The search for a model that meets the criteria for a holistic mechanistic model for SrtA catalysis led us to consider the possibility of reverse protonation. This type of mechanism has been invoked for an increasing number of enzymes, including fumarase, malic enzyme, thermolysin, β-xylosidase, and enolase which employ acid or base catalysis in the forward or reverse reaction (*45*, *59*−*62*). The underlying principle is that when two ionizable groups are required for catalysis and a bell-shaped pH−rate profile indicates that one residue must be protonated and the other deprotonated for activity, it is not possible to determine on the basis of the pH−rate profile alone what their respective protonation states are in the active form of the enzyme (*60*, *62*). Although at physiological pH the majority of the enzyme population will exist with the group with a lower pK_a deprotonated and the group with a higher pK_a protonated, there is an equilibrium in which a minor amount of enzyme exists in the reverse protonation state; i.e., the group with the lower pK_a is protonated and the group with the higher pK_a is deprotonated. Since the pH region of overlap of the protonated residue with the lower pK_a and the deprotonated residue with the higher pK_a corresponds to a bell shape, normal and reverse protonation states will yield pH−rate profiles that are identical in shape and yield the same pK_a values (*60*). However, when the active form of the enzyme is reverse protonated, the active enzyme represents a minor component of the total enzyme present and the catalytic efficiency will appear to be artificially depressed.

The principle of reverse protonation as it applies to SrtA is illustrated by Figure 10A, where the region of overlap of protonated His with a pK_a of 6.2 and deprotonated Cys with a pK_a of 9.4 corresponds to a bell-shaped region with the same pK_a values observed for SrtA. The fraction of enzyme in the reverse protonated form can be estimated to be $10^{-\Delta pK_a}$; for SrtA, this corresponds to approximately 0.06% (*63*). When the low catalytic efficiency observed for SrtA (75 M^{-1} s^{-1}) is corrected for the concentration of active enzyme in the reverse protonated form, the catalytic efficiency becomes approximately 10^5 M^{-1} s^{-1}. Since this value is still well below the diffusion limit and represents an activity level more comparable to that of other cysteine hydrolases, it seems reasonable to consider a reverse protonation model for SrtA catalysis. The phenomenon of reverse protonation also offers an explanation for the millimolar K_m observed for the Abz-LPETG-Dap(Dnp) SrtA substrate. Because such a minor percentage of the total enzyme is in an active form, the binding of substrate to inactive enzyme is expected to yield a higher apparent K_m value (*60*). Hence, unlike all previously proposed models, a reverse protonation model for SrtA would satisfy criterion 1.

A reverse protonation model for SrtA catalysis is also likely to satisfy criteria 2−7. Because of the inverse fractionation factor of the Cys sulfhydryl, D_2O is expected to shift the thiol−thiolate equilibrium more in the favor of the thiolate (*49*). Thus, in a D_2O environment, the percentage of SrtA present in active reverse protonated form with respect to Cys184 is increased, accounting for the observed inverse equilibrium isotope effect and in turn satisfying criterion 2. Furthermore, if the attack of the Cys184 thiolate on the peptide substrate is rate-limiting in the acylation reaction, proton inventories reflecting the inverse isotope effect and implicating one exchangeable hydrogenic site are expected, meeting criterion 3. If the reverse protonated enzyme is solely responsible for catalytic activity, the activity of SrtA must drop off at high and low pH since correctly protonated

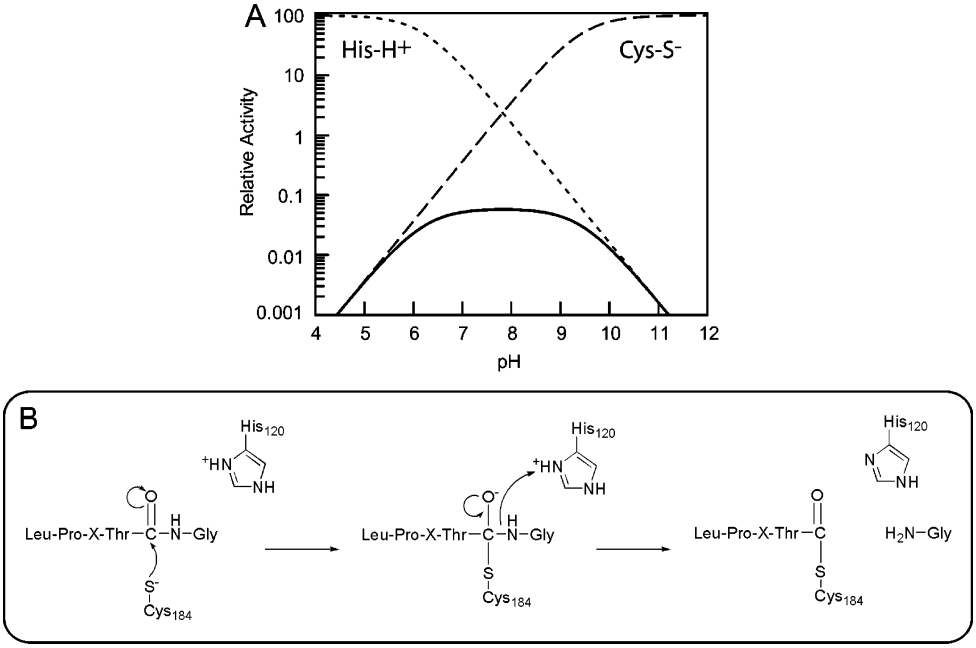

FIGURE 10: Reverse protonation model for SrtA-catalyzed transpeptidation. (A) Simulated SrtA activity profile invoking reverse protonation of Cys184 and His120. The relative activity is plotted on a log scale as a function of pH. The bell-shaped activity profile observed for SrtA (—), with pK_a values of 6.2 and 9.4, fits within the region of overlap of protonated His (- - -) and deprotonated Cys (— — —) with the corresponding pK_a's. (B) Reverse protonation mechanism for SrtA acylation. The LPXTG substrate binds to active SrtA in which Cys184 and His120 are reverse protonated; this form represents a minor fraction of the total SrtA population. The nucleophilic Cys184 thiolate attacks the carbonyl of the scissile Thr—Gly bond which results in the formation of a short-lived tetrahedral intermediate. His120 is hypothesized to protonate the substrate leaving group, facilitating the collapse of the tetrahedral intermediate and formation of the acyl—enzyme intermediate.

enzyme will not exist at extreme pH, satisfying criterion 4. Criteria 5—7 invoking the participation of oppositely protonated His120 and Cys184, with the majority of Cys184 existing as the undissociated thiol, are also implicit in a reverse protonation model for SrtA acylation.

To satisfy criterion 8 and the observation that His120 does not modulate the reactivity of Cys184 toward iodoacetamide, protonated His120 must play an essential role in SrtA acylation that is independent of Cys184. We therefore suggest that His120 functions as a general acid in catalysis to protonate the substrate leaving group after formation of the tetrahedral intermediate. Additionally, since we observe an inverse isotope effect on the SrtA reaction which can be explained by the involvement of Cys184 in the rate-limiting step of acylation, protonation of the substrate leaving group and collapse of the tetrahedral transition state must be fast relative to its formation. It is also interesting to note that the proposal of an essential role for His120 that is not related to mediating the activity of Cys184 may be consistent with the structural observations that the His120 side chain points away from Cys184 in the NMR structure of SrtA and is more than 10 Å from the modeled side chain of Cys184 in the crystal structure of SrtAC184A complexed with LPETG (*24*, *26*).

On the basis of these experimental data and the above discussion, we propose that the active form of SrtA is indeed reverse protonated and represents a minor percentage of the total enzyme. The proposed catalytic mechanism for SrtA acylation that invokes reverse protonation of His120 and Cys184 and satisfies all eight of the properties revealed in this study is shown in Figure 10B. The nucleophilic Cys184 thiolate attacks the carbonyl of the scissile Thr—Gly bond in the LPXTG-containing substrate, resulting in the formation of a short-lived tetrahedral intermediate. His120 is hypothesized to protonate the substrate leaving group, facilitating the collapse of the tetrahedral intermediate and formation of the acyl—enzyme intermediate. This model differs from the classical ion pair mechanism observed for papain in two respects. First, the active form of SrtA is a minor percentage of the total enzyme present, whereas in papain, the Cys—His ion pair is the major enzyme form (*64*). Second, in papain, the persistence of the thiolate anion at pH as low as 3 is directly coupled to the presence of the imidazolium counterion, whereas in SrtA, the Cys184 thiolate does not persist at abnormally low pH and its ionization state is considered independent of His120 protonation (*65*).

In conclusion, a novel mechanism for SrtA catalysis is proposed that differs from aspects of all three previously suggested models while maintaining consistency with reported structural and mechanistic findings. The results presented here thus lay a solid foundation for the further evaluation of SrtA elements involved in substrate binding and transition-state stabilization to enable the future development of highly potent and selective inactivators of the SrtA reaction with potential for in vivo efficacy. Such inhibitors may find promise as new therapeutics for preventing or significantly reducing the severity of infections caused by Gram-positive pathogens that are resistant to one or more antibiotics.

ACKNOWLEDGMENT

We gratefully acknowledge Drs. Stewart Fisher and Gunter Kern of AstraZeneca Pharmaceuticals for their kind assistance with pre-steady-state experiments. We also thank the thoughtful contributions of the referees to the manuscript.

REFERENCES

1. Mazmanian, S. K., Liu, G., Ton-That, H., and Schneewind, O. (1999) *Staphylococcus aureus* sortase, an enzyme that anchors surface proteins to the cell wall, *Science 285*, 760−3.
2. Perry, A. M., Ton-That, H., Mazmanian, S. K., and Schneewind, O. (2002) Anchoring of surface proteins to the cell wall of *Staphylococcus aureus*. III. Lipid II is an *in vivo* peptidoglycan substrate for sortase-catalyzed surface protein anchoring, *J. Biol. Chem. 277*, 16241−8.
3. Ruzin, A., Severin, A., Ritacco, F., Tabei, K., Singh, G., Bradford, P. A., Siegel, M. M., Projan, S. J., and Shlaes, D. M. (2002) Further evidence that a cell wall precursor [C(55)-MurNAc-(peptide)-GlcNAc] serves as an acceptor in a sorting reaction, *J. Bacteriol. 184*, 2141−7.
4. Pallen, M. J., Lam, A. C., Antonio, M., and Dunbar, K. (2001) An embarrassment of sortases: A richness of substrates? *Trends Microbiol. 9*, 97−102.
5. Comfort, D., and Clubb, R. T. (2004) A comparative genome analysis identifies distinct sorting pathways in Gram-positive bacteria, *Infect. Immun. 72*, 2710−22.
6. Mazmanian, S. K., Ton-That, H., Su, K., and Schneewind, O. (2002) An iron-regulated sortase anchors a class of surface protein during *Staphylococcus aureus* pathogenesis, *Proc. Natl. Acad. Sci. U.S.A. 99*, 2293−8.
7. Mazmanian, S. K., Liu, G., Jensen, E. R., Lenoy, E., and Schneewind, O. (2000) *Staphylococcus aureus* sortase mutants defective in the display of surface proteins and in the pathogenesis of animal infections, *Proc. Natl. Acad. Sci. U.S.A. 97*, 5510−5.
8. Bolken, T. C., Franke, C. A., Jones, K. F., Zeller, G. O., Jones, C. H., Dutton, E. K., and Hruby, D. E. (2001) Inactivation of the srtA gene in *Streptococcus gordonii* inhibits cell wall anchoring of surface proteins and decreases in vitro and in vivo adhesion, *Infect. Immun. 69*, 75−80.
9. Garandeau, C., Reglier-Poupet, H., Dubail, I., Beretti, J. L., Berche, P., and Charbit, A. (2002) The sortase SrtA of *Listeria monocytogenes* is involved in processing of internalin and in virulence, *Infect. Immun. 70*, 1382−90.
10. Osaki, M., Takamatsu, D., Shimoji, Y., and Sekizaki, T. (2002) Characterization of *Streptococcus suis* genes encoding proteins homologous to sortase of Gram-positive bacteria, *J. Bacteriol. 184*, 971−82.
11. Kharat, A. S., and Tomasz, A. (2003) Inactivation of the srtA gene affects localization of surface proteins and decreases adhesion of *Streptococcus pneumoniae* to human pharyngeal cells *in vitro*, *Infect. Immun. 71*, 2758−65.
12. Lee, S. F., and Boran, T. L. (2003) Roles of sortase in surface expression of the major protein adhesin P1, saliva-induced aggregation and adherence, and cariogenicity of *Streptococcus mutans*, *Infect. Immun. 71*, 676−81.
13. Barnett, T. C., and Scott, J. R. (2002) Differential recognition of surface proteins in *Streptococcus pyogenes* by two sortase gene homologs, *J. Bacteriol. 184*, 2181−91.
14. Scott, C. J., McDowell, A., Martin, S. L., Lynas, J. F., Vandenbroeck, K., and Walker, B. (2002) Irreversible inhibition of the bacterial cysteine protease-transpeptidase sortase (SrtA) by substrate-derived affinity labels, *Biochem. J. 366*, 953−8.
15. Connolly, K. M., Smith, B. T., Pilpa, R., Ilangovan, U., Jung, M. E., and Clubb, R. T. (2003) Sortase from *S. aureus* does not contain a thiolate-imidazolium ion pair in its active site, *J. Biol. Chem. 24*, 24.
16. Kruger, R. G., Barkallah, S., Frankel, B. A., and McCafferty, D. G. (2004) Inhibition of the *Staphylococcus aureus* sortase transpeptidase SrtA by phosphinic peptidomimetics, *Bioorg. Med. Chem. 12*, 3723−9.
17. Liew, C. K., Smith, B. T., Pilpa, R., Suree, N., Ilangovan, U., Connolly, K. M., Jung, M. E., and Clubb, R. T. (2004) Localization and mutagenesis of the sorting signal binding site on sortase A from *Staphylococcus aureus*, *FEBS Lett. 571*, 221−6.
18. Kim, S. H., Shin, D. S., Oh, M. N., Chung, S. C., Lee, J. S., Chang, I. M., and Oh, K. B. (2003) Inhibition of sortase, a bacterial surface protein anchoring transpeptidase, by β-sitosterol-3-O-glucopyranoside from *Fritillaria verticillata*, *Biosci., Biotechnol., Biochem. 67*, 2477−9.
19. Kim, S. H., Shin, D. S., Oh, M. N., Chung, S. C., Lee, J. S., and Oh, K. B. (2004) Inhibition of the bacterial surface protein anchoring transpeptidase sortase by isoquinoline alkaloids, *Biosci., Biotechnol., Biochem. 68*, 421−4.
20. Kim, S. W., Chang, I. M., and Oh, K. B. (2002) Inhibition of the bacterial surface protein anchoring transpeptidase sortase by medicinal plants, *Biosci., Biotechnol., Biochem. 66*, 2751−4.
21. Frankel, B. A., Bentley, M., Kruger, R. G., and McCafferty, D. G. (2004) Vinyl Sulfones: Inhibitors of SrtA, a transpeptidase required for cell wall protein anchoring and virulence in *Staphylococcus aureus*, *J. Am. Chem. Soc. 126*, 3404−5.
22. Ton-That, H., and Schneewind, O. (1999) Anchor structure of staphylococcal surface proteins. IV. Inhibitors of the cell wall sorting reaction, *J. Biol. Chem. 274*, 24316−20.
23. Oh, K. B., Kim, S. H., Lee, J., Cho, W. J., Lee, T., and Kim, S. (2004) Discovery of diarylacrylonitriles as a novel series of small molecule sortase A inhibitors, *J. Med. Chem. 47*, 2418−21.
24. Ilangovan, U., Ton-That, H., Iwahara, J., Schneewind, O., and Clubb, R. T. (2001) Structure of sortase, the transpeptidase that anchors proteins to the cell wall of *Staphylococcus aureus*, *Proc. Natl. Acad. Sci. U.S.A. 98*, 6056−61.
25. Ton-That, H., Mazmanian, S. K., Alksne, L., and Schneewind, O. (2002) Anchoring of surface proteins to the cell wall of *Staphylococcus aureus*. Cysteine 184 and histidine 120 of sortase form a thiolate-imidazolium ion pair for catalysis, *J. Biol. Chem. 277*, 7447−52.
26. Zong, Y., Bice, T. W., Ton-That, H., Schneewind, O., and Narayana, S. V. (2004) Crystal structures of *Staphylococcus aureus* sortase A and its substrate complex, *J. Biol. Chem. 279*, 31383−9.
27. Zong, Y., Mazmanian, S. K., Schneewind, O., and Narayana, S. V. (2004) The structure of sortase B, a cysteine transpeptidase that tethers surface protein to the *Staphylococcus aureus* cell wall, *Structure 12*, 105−12.
28. Zhang, R., Wu, R., Joachimiak, G., Mazmanian, S. K., Missiakas, D. M., Gornicki, P., Schneewind, O., and Joachimiak, A. (2004) Structures of sortase B from *Staphylococcus aureus* and *Bacillus anthracis* reveal catalytic amino acid triad in the active site, *Structure 12*, 1147−56.
29. Huang, X., Aulabaugh, A., Ding, W., Kapoor, B., Alksne, L., Tabei, K., and Ellestad, G. (2003) Kinetic mechanism of *Staphylococcus aureus* sortase SrtA, *Biochemistry 42*, 11307−15.
30. Kruger, R. G., Dostal, P., and McCafferty, D. G. (2004) Development of a high-performance liquid chromatography assay and revision of kinetic parameters for the *Staphylococcus aureus* sortase transpeptidase SrtA, *Anal. Biochem. 326*, 42−8.
31. Kruger, R. G., Otvos, B., Frankel, B. A., Bentley, M., Dostal, P., and McCafferty, D. G. (2004) Analysis of the substrate specificity of the *Staphylococcus aureus* sortase transpeptidase SrtA, *Biochemistry 43*, 1541−51.
32. Segel, I. H. (1975) *Enzyme kinetics: Behavior and analysis of rapid equilibrium and steady-state systems*, Wiley, New York.
33. Varon, R., Garcia-Sevilla, F., Garcia-Moreno, M., Garcia-Canovas, F., Peyro, R., and Duggleby, R. G. (1997) Computer program for the equations describing the steady state of enzyme reactions, *Comput. Appl. Biosci. 13*, 159−67.
34. Karkowsky, A. M., Bergamini, M. V., and Orlowski, M. (1976) Kinetic studies of sheep kidney γ-glutamyl transpeptidase, *J. Biol. Chem. 251*, 4736−43.
35. Patrie, S. M., Charlebois, J. P., Whipple, D., Hendrickson, C. L., Quinn, J. P., Marshall, A. G., Mukhopadhyay, B., Kelleher, N. L. (2004) Construction of a hybrid quadrupole/Fourier-transform mass spectrometer for versatile MS/MS above 10 kDa, *J. Am. Soc. Mass Spectrom. 15*, 1099−1108.
36. Marshall, A. G., Wang, T. C. L., and Ricca, T. L. (1985) Tailored excitation for Fourier-transform ion cyclotron mass spectrometry, *J. Am. Chem. Soc. 107*, 7893−7.
37. Little, D. P., Speir, J. P., Senko, M. W., O'Connor, P. B., and McLafferty, F. W. (1994) Infrared multiphoton dissociation of large multiply charged ions for biomolecule sequencing, *Anal. Chem. 66*, 2809−15.
38. Horn, D. M., Zubarev, R. A., and McLafferty, F. W. (2000) Automated reduction and interpretation of high-resolution electrospray mass spectra of large molecules, *J. Am. Soc. Mass Spectrom. 11*, 320−32.
39. Taylor, G. K., Kim, Y. B., Forbes, A. J., Meng, F., McCarthy, R., and Kelleher, N. L. (2003) Web and database software for identification of intact proteins using "top down" mass spectrometry, *Anal. Chem. 75*, 4081−6.
40. Kitz, R., and Wilson, I. B. (1962) Esters of methanesulfonic acid as irreversible inhibitors of acetylcholinesterase, *J. Biol. Chem. 237*, 3245−9.

41. Ton-That, H., Liu, G., Mazmanian, S. K., Faull, K. F., and Schneewind, O. (1999) Purification and characterization of sortase, the transpeptidase that cleaves surface proteins of *Staphylococcus aureus* at the LPXTG motif, *Proc. Natl. Acad. Sci. U.S.A. 96*, 12424−9.
42. Chung, S. I., and Folk, J. E. (1972) Kinetic studies with transglutaminases. The human blood enzymes activated coagulation factor 13 and the guinea pig hair follicle enzyme, *J. Biol. Chem. 247*, 2798−807.
43. Arion, W. J., and Nordlie, R. C. (1964) Liver microsomal glucose 6-phosphatase, inorganic pyrophosphatase, and pyrophosphate-glucose phosphotransferase. II. Kinetic studies, *J. Biol. Chem. 239*, 2752−7.
44. Cornish-Bowden, A. (1995) *Fundamentals of Enzyme Kinetics*, Portland Press, London.
45. Mock, W. L., and Stanford, D. J. (1996) Arazoformyl dipeptide substrates for thermolysin. Confirmation of a reverse protonation catalytic mechanism, *Biochemistry 35*, 7369−77.
46. Pinitglang, S., Watts, A. B., Patel, M., Reid, J. D., Noble, M. A., Gul, S., Bokth, A., Naeem, A., Patel, H., Thomas, E. W., Sreedharan, S. K., Verma, C., and Brocklehurst, K. (1997) A classical enzyme active center motif lacks catalytic competence until modulated electrostatically, *Biochemistry 36*, 9968−82.
47. Whitaker, J. R., and Bender, M. L. (1965) Kinetics of papain-catalyzed hydrolysis of α-N-benzoyl-L-arginine ethyl ester and α-N-benzoyl-L-argininamide, *J. Am. Chem. Soc. 87*, 2728−37.
48. Sarkany, Z., Szeltner, Z., and Polgar, L. (2001) Thiolate-imidazolium ion pair is not an obligatory catalytic entity of cysteine peptidases: The active site of picornain 3C, *Biochemistry 40*, 10601−6.
49. Schowen, R. L. (1977) Solvent isotope effects on enzymic reactions, in *Isotope effects on enzyme-catalyzed reactions* (Cleland, W. W., OLeary, M. H., and Northrop, D. B., Eds.) pp 64−99, University Park Press, Baltimore.
50. Venkatasubban, K. S., and Schowen, R. L. (1984) The proton inventory technique, *CRC Crit. Rev. Biochem. 17*, 1−44.
51. Sarkany, Z., Skern, T., and Polgar, L. (2000) Characterization of the active site thiol group of rhinovirus 2A proteinase, *FEBS Lett. 481*, 289−92.
52. Storer, A. C., and Menard, R. (1994) Catalytic mechanism in papain family of cysteine peptidases, *Methods Enzymol. 244*, 486−500.
53. Dessen, A. (2004) A new catalytic dyad regulates anchoring of molecules to the Gram-positive cell wall by sortases, *Structure 12*, 6−7.
54. Hedstrom, L. (2002) Serine protease mechanism and specificity, *Chem. Rev. 102*, 4501−24.
55. Wang, H., Vath, G. M., Gleason, K. J., Hanna, P. E., and Wagner, C. R. (2004) Probing the mechanism of hamster arylamine *N*-acetyltransferase 2 acetylation by active site modification, site-directed mutagenesis, and pre-steady state and steady-state kinetic studies, *Biochemistry 43*, 8234−46.
56. Sfakianos, M. K., Wilson, L., Sakalian, M., Falany, C. N., and Barnes, S. (2002) Conserved residues in the putative catalytic triad of human bile acid coenzyme A:amino acid N-acyltransferase, *J. Biol. Chem. 277*, 47270−5.
57. Sarkany, Z., and Polgar, L. (2003) The unusual catalytic triad of poliovirus protease 3C, *Biochemistry 42*, 516−22.
58. Marraffini, L. A., Ton-That, H., Zong, Y., Narayana, S. V., and Schneewind, O. (2004) Anchoring of surface proteins to the cell wall of *Staphylococcus aureus*. A conserved arginine residue is required for efficient catalysis of sortase A, *J. Biol. Chem. 279*, 37763−70.
59. Sims, P. A., Larsen, T. M., Poyner, R. R., Cleland, W. W., and Reed, G. H. (2003) Reverse protonation is the key to general acid−base catalysis in enolase, *Biochemistry 42*, 8298−306.
60. Cleland, W. W. (1977) Determining the chemical mechanisms of enzyme-catalyzed reactions by kinetic studies, *Adv. Enzymol. Relat. Areas Mol. Biol. 45*, 273−387.
61. Vocadlo, D. J., Wicki, J., Rupitz, K., and Withers, S. G. (2002) A case for reverse protonation: Identification of Glu160 as an acid/base catalyst in *Thermoanaerobacterium saccharolyticum* β-xylosidase and detailed kinetic analysis of a site-directed mutant, *Biochemistry 41*, 9736−46.
62. Nuiry, I. I., and Cook, P. F. (1985) The pH dependence of the reductive carboxylation of pyruvate by malic enzyme, *Biochim. Biophys. Acta 829*, 295−8.
63. Price, N. E., and Cook, P. F. (1996) Kinetic and chemical mechanisms of the sheep liver 6-phosphogluconate dehydrogenase, *Arch. Biochem. Biophys. 336*, 215−23.
64. Polgar, L. (1973) On the mode of activation of the catalytically essential sulfhydryl group of papain, *Eur. J. Biochem. 33*, 104−9.
65. Polgar, L. (1974) Mercaptide-imidazolium ion-pair: The reactive nucleophile in papain catalysis, *FEBS Lett. 47*, 15−8.

BI050141J